minerals

MDPI

Article

Separation of Fe from Mn in the Cryogenian Sedimentary Mn Deposit, South China: Insights from Ore Mineral Chemistry and S Isotopes from the Dawu Deposit

Zhiming Xu [1,2], Chengquan Wu [1,*], Zhengwei Zhang [1], Jinhong Xu [1,3], Xiyao Li [1,3] and Ziru Jin [1,3]

[1] State Key Laboratory of Ore Deposit Geochemistry, Institute of Geochemistry, Chinese Academy of Sciences, Guiyang 550081, China; xuzhimingfzu@163.com (Z.X.); zhangzhengwei@mail.gyig.ac.cn (Z.Z.); xujinhong@mail.gyig.ac.cn (J.X.); lixiyao@mail.gyig.ac.cn (X.L.); jinziru@mail.gyig.ac.cn (Z.J.)
[2] Fuzhou University, Fuzhou 350108, China
[3] College of Earth and Planetary Sciences, University of Chinese Academy of Sciences, Beijing 100049, China
* Correspondence: wuchengquan@mail.gyig.ac.cn

Abstract: Manganese and Fe have similar geochemical properties in the supergene environment. Separation of Mn and Fe is an important process for the formation of high-grade sedimentary manganese deposits. Large-scale manganese carbonate deposits (total reserves of approximately 700 Mt) were formed during the interglacial of the Sturtian and Marinoan in South China. The orebodies are hosted in the black rock series at the basal Datangpo Formation of the Cryogenian period. The Fe contents in ores range from 1.15 to 7.18 wt.%, with an average of 2.80 wt.%, and the average Mn/Fe ratio is 8.9, indicating a complete separation of Mn and Fe during the formation of manganese ores. Here, we present element data of manganese carbonates and sulfur isotopes of pyrite from the Dawu deposit, Guizhou, China, aiming to investigate the separation mechanism of Mn and Fe and the ore genesis. The Fe in ores mainly occurs as carbonate ($FeCO_3$) and pyrite (FeS_2). The Mn, Ca, Mg and Fe exist in the form of isomorphic substitutions in manganese carbonate. The contents of $FeCO_3$ in manganese carbonates are similar in different deposits, with averages of 2.6–2.8 wt.%. The whole-rock Fe and S contents have an obvious positive correlation (R = 0.69), indicating that the difference of whole-rock Fe content mainly comes from the pyrite content. The $\delta^{34}S_{V\text{-}CDT}$ of pyrite varies from 40.0 to 48.3‰, indicating that the pyrite formed in a restricted basin where sulfate supply was insufficient and the sulfate concentrations were extremely low. Additionally, the whole-rock Fe content is negatively correlated with the $\delta^{34}S$ values of the whole-rock and pyrite, with correlation coefficients of −0.78 and −0.83, respectively. Two stages of separations of Mn and Fe might have occurred during the mineralization processes. The reduced seawater became oxidized gradually after the Sturtian glaciation, and Fe^{2+} was oxidized and precipitated before Mn^{2+}, which resulted in the first-stage separation of Mn and Fe. The residual Mn-rich and Fe-poor seawater flowed into the restricted rift basin. Mn and Fe were then precipitated in sediments as oxyhydroxide as the seawater was oxidized. At the early stage of diagenesis, organic matter was oxidized, and manganese oxyhydroxide was reduced, forming the manganese carbonate. H_2S was insufficient in the restricted basin due to the extremely low sulfate concentration. The Fe^{2+} was re-released due to the lack of H_2S, resulting in the second-stage separation of Mn and Fe. Finally, the manganese carbonate deposit with low Fe and very high $\delta^{34}S$ was formed in the restricted basin after the Sturtian glaciation.

Keywords: separation of Mn and Fe; Cryogenian manganese deposit; marine redox; sulfur isotope; South China

Citation: Xu, Z.; Wu, C.; Zhang, Z.; Xu, J.; Li, X.; Jin, Z. Separation of Fe from Mn in the Cryogenian Sedimentary Mn Deposit, South China: Insights from Ore Mineral Chemistry and S Isotopes from the Dawu Deposit. *Minerals* **2021**, *11*, 446. https://doi.org/10.3390/min11050446

Academic Editor: Panagiotis Voudouris

Received: 9 March 2021
Accepted: 20 April 2021
Published: 23 April 2021

1. Introduction

The abundance of Fe in the continental crust is 7.08 wt.%, which is much higher than that of Mn at 0.14 wt.% [1]. Separation of Mn and Fe is very common in sedimentary

manganese deposits [2–4], such as the Archean Noamundi Fe-Mn deposit in India, the Late Proterozoic Otjosond Mn-Fe deposit in Namibia, the Neoproterozoic Urucum Fe-Mn deposit in Brazil, and the Eocene Elazığ-Malatya Fe-Mn deposit in eastern Turkey [5–9]. The area of stability of Mn^{2+} is larger than that of Fe^{2+} under supergene conditions [9,10]. In a reduced environment, Mn and Fe are dissolved in water in the form of Mn^{2+} and Fe^{2+}, respectively, and Fe^{2+} is oxidized and precipitated before Mn^{2+} in the process of gradual oxidation [10]. Moreover, in the anoxic and sulfur-rich environment, Mn occurs as soluble manganese bicarbonate and manganese sulfide with poor stability, while Fe mainly occurs as stable sulfide [10,11]. Furthermore, some microorganisms selectively promote manganese oxidation and may result in the separation of Mn and Fe [10–12]. Therefore, the study of the separation of Mn and Fe can trace the Mn mineralization process and deepen the understanding of ore genesis.

The Cryogenian (also known as the Nanhua period in China) manganese deposits in South China are mainly concentrated in the adjacent area of Guizhou, Hunan, Chongqing, and Hubei [13]. Four super-large (Mn reserves >100 Mt) manganese deposits have been discovered since 2008, with the total Mn resources exceeding 700 Mt [13–15]. The orebodies occur in the black rock series at the basal Datangpo Formation of the Cryogenian System, and the ore minerals are mainly manganese carbonates [13,14,16]. Previous studies have shown that the Cryogenian manganese deposits were formed in the restricted basins, and the Mn was precipitated as oxyhydroxide and was then reduced to carbonates [13]. After the Sturtian glaciation, the basin was in a redox stratified environment in the Datangpo stage. The bottom seawater was in a reductive state, where it was conducive to the enrichment of Fe and Mn, while the upper ocean was in an oxidizing environment, which led to precipitation of Fe and Mn [13]. The gradually oxidized environment was favorable for the separation of Fe from Mn. The whole-rock Fe contents of ores are 1.15–7.18 wt.%, with an average of 2.80 wt.%, and the Mn/Fe ratios are 1.9–26.4, indicating that there may be a complete separation of Mn and Fe during the formation of manganese ore [13]. However, the separation process and its control mechanism are still unclear. Here, we present element data of manganese carbonates and in situ sulfur isotopes of pyrite from the Dawu manganese deposit in Guizhou, South China, aiming to investigate the separation mechanism of Mn and Fe and to further understand the genesis of the deposit.

2. Geological Setting

The study area is located at the conjunction of the Yangtze Block and Jiangnan Orogen (Figure 2A). The Yangtze Plate and Cathaysia Plate merged into the South China Plate at ~1.1–0.9 Ga ago due to the Sibao Orogeny (also known as the Jinning Movement or Jiangnan Movement) [17–19]. The South China Plate began to break off at ~820 Ma, forming the Nanhua rift [20–23]. At that time, the southeastern part of the Yangtze Platform was situated on a passive continental margin, and a large number of basins were formed along the rift, which provided the advantageous space for deposition of Neoproterozoic lithologies [21,24,25]. The study area was mainly a rift basin (Nanhua basin) during the Cryogenian period, which evolved into shelf, platform, passive continental margin, or continental margin slope in the Sinian period [26], providing a stable tectonic environment for the formation of manganese deposits.

The Neoproterozoic strata are widely distributed in the study area, gradually changing from basinal facies in eastern Guizhou and western Hunan to transition facies and platform facies in the north and west [27]. The Datangpo Formation with manganese carbonate is distributed in both basinal and transitional facies. The underlying stratum is the Tiesi'ao Formation, and the overlying stratum is the Nantuo Formation (Figure 1), all of which with conformable contact. The zircon U-Pb ages of the tuff interlayers at the bottom and top of the Datangpo Formation are 662.9 ± 4.3 Ma [27] and 654.5 ± 3.8 Ma [28], respectively, constraining the sedimentary age of Datangpo Formation. The Tiesi'ao Formation and Nantuo Formation are glacial sedimentary strata [27], corresponding to the Sturtian and Marinoan glacial sedimentary strata of the Cryogenian System [27,29–33]. The thickness of

the Datangpo Formation in the study area is approximately 200–500 m, with dark gray and grayish-yellow silty shale in the upper part and black carbonaceous shale in the lower part (Figure 1). The manganese carbonate orebody occurs in the black shale of the first member of the Datangpo Formation (Figure 1).

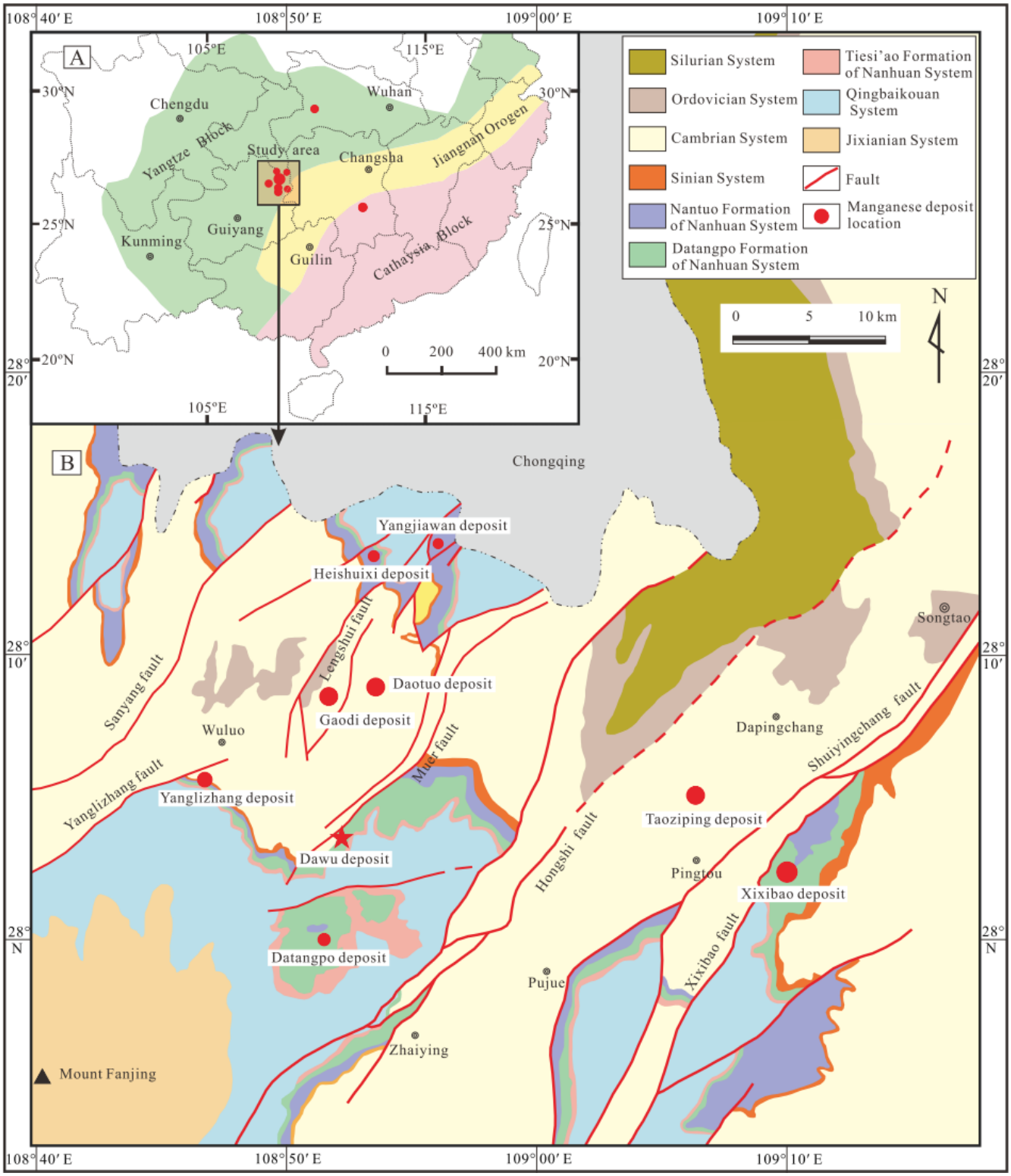

Figure 1. (**A**) Tectonic sketch map of South China and the location of the study area. (**B**) Geological sketch map of the Cryogenian manganese deposits in eastern Guizhou, China (modified from [13,33]).

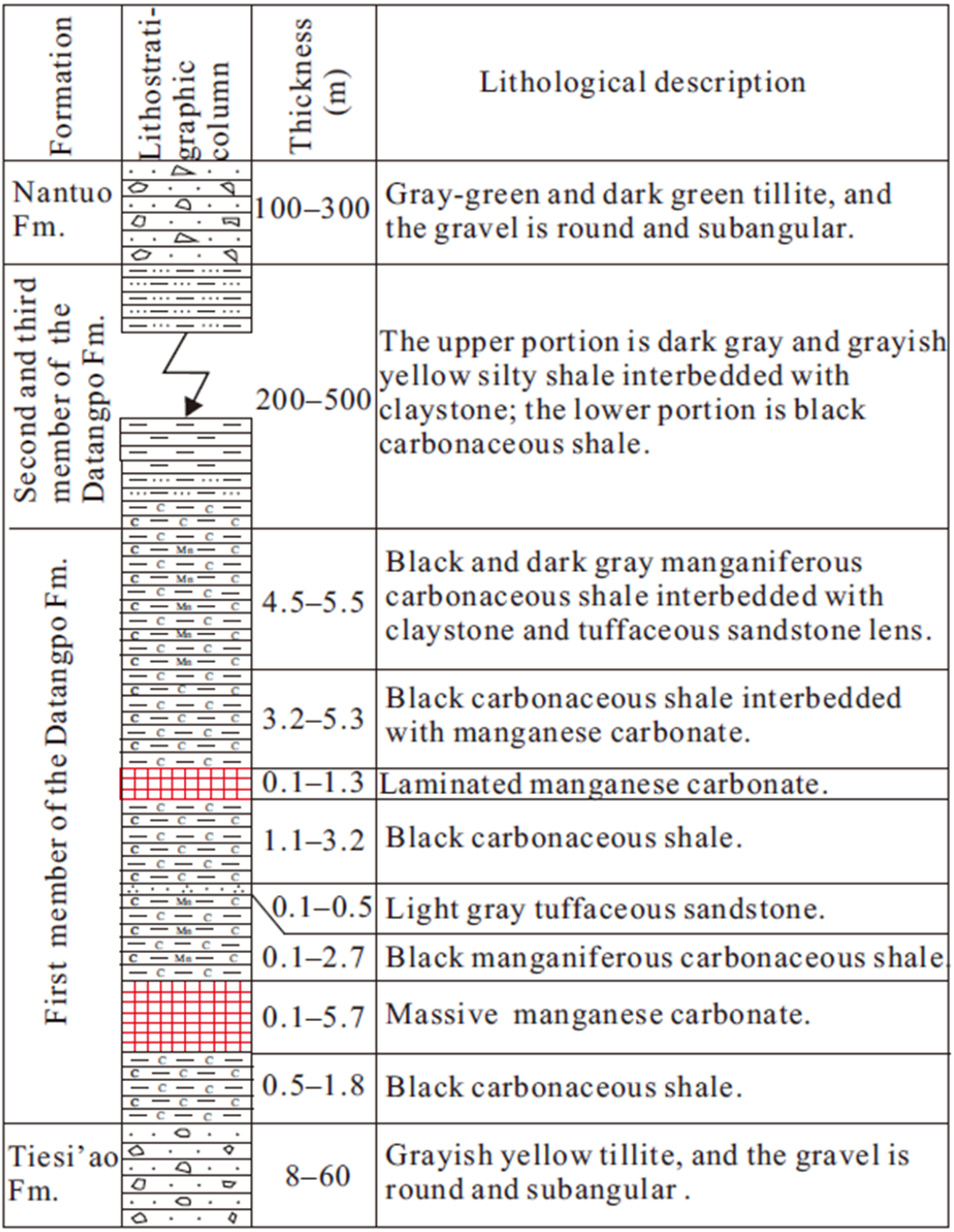

Figure 2. Stratigraphic details for the Datangpo Formation in eastern Guizhou, China (modified from [13]).

3. Deposit Descriptions

The Cryogenian manganese carbonate deposits are distributed in Guizhou, Hunan, Chongqing, and Hubei, and are mainly concentrated in eastern Guizhou (Figure 2). The typical deposits include Yanglizhang, Dawu, Datangpo, Daotuo, Xixibao, Gaodi, and

Taoziping deposits in Guizhou (Figure 2B); Rongxi deposit in Chongqing; Minle, Gucheng, and Xiangtan deposits in Hunan; and Gucheng deposit in Hubei [13,14,33].

The manganese-bearing rock series is the black rock series of the first member of the Datangpo Formation, which is mainly composed of manganese carbonate, black carbonaceous shale, manganiferous carbonaceous shale, and tuffaceous sandstone (Figures 1, 3 and 4A). The thickness of the manganese-bearing rock series is generally 14–30 m and is positively correlated with that of manganese carbonate orebodies [14,34]. The lithology of the manganese-bearing rock series displays a zonal distribution, with a manganese carbonate belt, a carbonaceous shale-manganese-dolomite belt, and a carbonaceous shale-silty carbonaceous shale belt from the center to the edge of the sedimentary basin [34–36]. The thickness of the manganese-bearing rock series in the Dawu deposit is 13.0−28.4 m, with an average of 18.0 m [34].

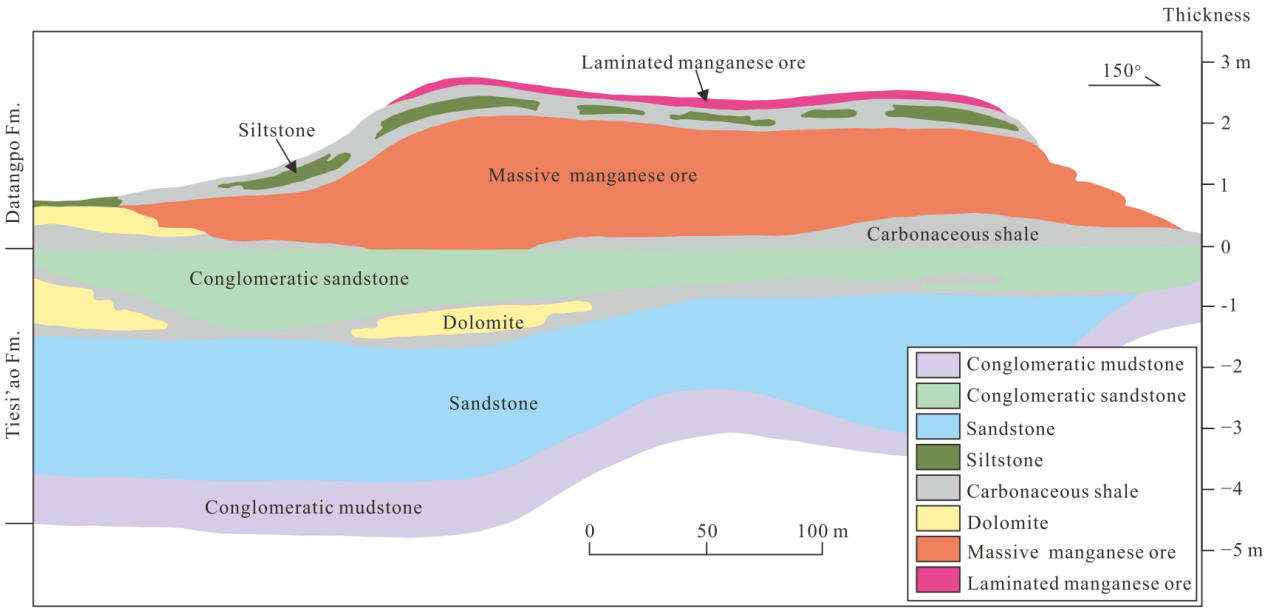

Figure 3. The geological section along exploration line 51 in the Dawu deposit (modified from [37,38]).

The manganese-bearing rock series commonly has 2–3 manganese carbonate layers. The orebodies are stratified and lenticular, and the occurrences are consistent with those of wall rocks (Figure 3). The thickness of the orebody varies greatly, generally ranging from 1 to 5 m. From the center to the edge of the sedimentary basin, the thickness of the orebody gradually becomes thinner, and the number of ore layers gradually decreases. The orebodies are separated by carbonaceous shale, carbonaceous claystone, and tuffaceous sandstone. The wall rocks are mainly black carbonaceous shale (Figures 3 and 4B,C). The orebody of the Dawu deposit is stratified, with approximately 5500 m in length and 500 m in width. The orebody is 0.5–3.1 m thick, with an average of 1.4 m [34]. The upper orebody is 0.19–0.25 m thick, the lower orebody is 0.74–1.64 m thick, and the orebodies are separated by 0.17–0.86 m thick siltstone and shale (Figure 3) [37].

The ore minerals are mainly Ca-rhodochrosite and Mn-calcite. The gangue minerals are mainly quartz, feldspar, muscovite, pyrite, montmorillonite, and illite, with minor apatite. The Ca-rhodochrosite mainly exhibits micrite and microcrystalline texture (Figure 4H,I), and the particle size is generally 2–6 μm. The cement between Ca-rhodochrosite particles is Mn-calcite, argillaceous mineral, and organic matter (Figure 4H,I). Pyrite is very common in the ores, exhibiting idiomorphic–hypidiomorphic granular and framboidal textures (Figure 4G,H). The ore structure is mainly massive (Figure 4D), laminated (Figure 4E,G), and banded (Figure 4F). The massive ore usually has high ore grade and is mainly composed of Ca-rhodochrosite and Mn-calcite, which is common in thick orebodies, and the organic concretions occur in some massive ores (Figure 4D). The lami-

nated ore is the most common, and the thin laminate is mainly composed of manganese carbonate, organic matter, and argillaceous minerals (Figure 4E,G). The ores are generally low-grade, low-Fe, and high-P type manganese carbonates, with 12–30 wt.% Mn (average 21.3 wt.%), 1.51–7.18 wt.% Fe (average 2.76 wt.%), and 0.06–1.27 wt.% P (average 0.22). The Mn/Fe ratios of ores range from 1.9 to 26.4 (average 8.9), and the P/Mn ratios range from 0.003 to 0.064 (average 0.011).

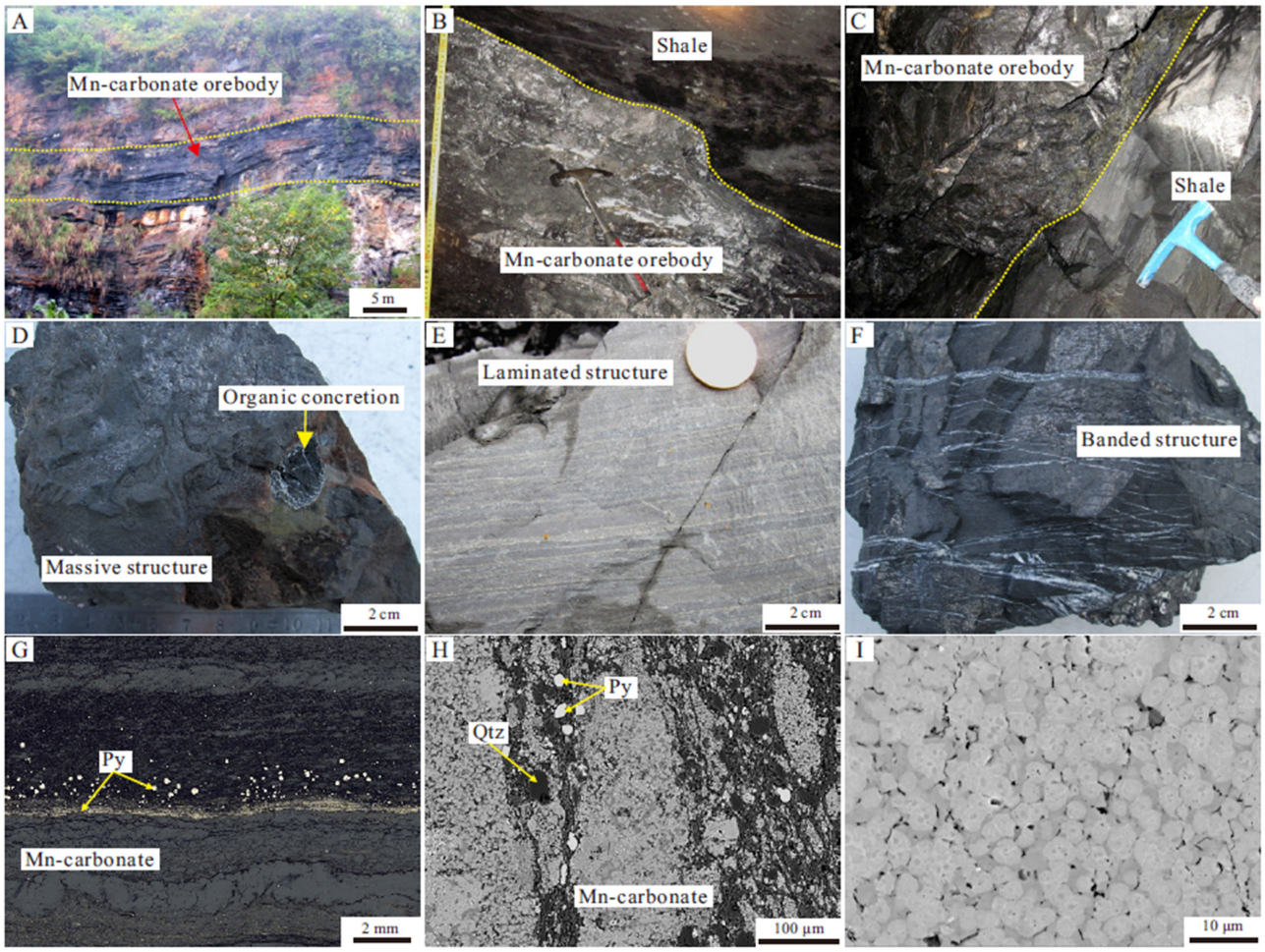

Figure 4. Manganese-bearing rock series, morphology of orebody, and ore structures of the Cryogenian manganese deposits in South China. (**A**) Manganese-bearing rock series occur in the first member of the Datangpo Formation; (**B**,**C**) manganese carbonate orebody and wall rock; (**D**) ore with massive structure and organic concretion; (**E**) laminated structure—the laminae are 0.1–3 mm and mainly composed of rhodochrosite, argillaceous minerals, and carbonaceous material; (**F**) banded structure; (**G**) laminated structure (reflected light); (**H**,**I**) micritic and microcrystalline manganese carbonates (BSE); Py—pyrite; Qtz—quartz.

4. Sampling and Analytical Methods

The samples were collected from the 640-tunnel of the Dawu mining area, with geographical coordinates of 28°02′43″ N, 108°51′34″ E.

Electron probe microanalysis (EPMA) of manganese carbonate was conducted using a JXA-5230F Plus Hyper Probe at State Key Laboratory of Ore Deposit Geochemistry, Institute of Geochemistry, Chinese Academy of Sciences (SKLODG, IGCAS), with the 5–10 μm beam diameter, 25 kV accelerating potential, and 10 nA probe current. Rhodochrosite, calcite, magnesite, and siderite were used as standards; all of the standards were tested for homogeneity before their utilization for quantitative analysis. The data were reduced using the ZAF correction method.

The in situ sulfur isotope measurements of pyrite were performed on a Nu Plasma III MC-ICP-MS (Multi-receiver plasma mass spectrometry, Nu Instruments) that was attached to a RESOlution-155 ArF193-nm laser ablation system (Australian Scientific Instruments) at SKLODG, IGCAS. The mass separation was calculated as 0.3333 in the analyses. The instrument was utilized in pseudo-medium resolution mode [39] to resolve polyatomic interferences from ^{16}O–^{16}O for ^{32}S and ^{16}O–^{18}O for ^{34}S, adjusting the source slit to medium (0.05 mm) in conjunction with using the alpha slit. Sulfide was ablated in a mixture of helium (350 mL/min) and nitrogen (2 mL/min) atmosphere using the following parameters: 20 s baseline time, 40 s ablation time, 40 s wash time, 60 μm spot size, 6 Hz repetition rate, and 2–3 J/cm^2 energy density. All analyses followed standard sample bracketing procedures of three samples bracketed by chalcopyrite pressed powder tablet (PSPT-1) [40,41]. Two natural pyrite crystals (SB-1 from the Shangbao W-Sn deposit and HYC-1 from the Huayangchuan Nb-U-REE deposit, China) were treated as quality control. The measured $\delta^{34}S_{V\text{-}CDT}$ for the standard was 16.57‰ (n = 12) for SB-1 and −5.76‰ for HYC-1(n = 12), which was identical to the recommended value (16.57‰ for SB-1 and −5.76‰ for HYC-1) (IRMS).

5. Results

The element data of manganese carbonate in the Dawu manganese deposit are shown in Table 1. The Mn, Ca, Mg and Fe exist in the form of isomorphic substitutions in manganese carbonate, forming Ca-rhodochrosite and Mn-calcite. The $MnCO_3$ is negatively correlated with $CaCO_3$ and $MgCO_3$, and the correlation coefficients are −0.98 and −0.73, respectively (Figure 5A,B). The $MnCO_3$ is positively correlated with P_2O_5, with a correlation coefficient of 0.64 (Figure 5D). The content of $FeCO_3$ in manganese carbonate ranges from 0.65 to 6.57 wt.%, with an average of 2.63 wt.%. There is no obvious correlation between $MnCO_3$ and $FeCO_3$ (Figure 5C).

Table 1. EPMA analyses of carbonates from the Dawu manganese deposit (wt.%).

Sample No.	Mineral	$MnCO_3$	$CaCO_3$	$MgCO_3$	$FeCO_3$	P_2O_5	Al_2O_3	SiO_2	Total
DW02-6-1	Ca-Rds	71.14	19.08	6.79	1.86	0.58	0.02	0.11	99.57
DW02-6-2	Ca-Rds	74.82	18.06	5.96	1.13	0.26	bld	0.03	100.26
DW02-6-3	Ca-Rds	54.58	29.20	8.61	4.35	0.18	0.03	0.45	97.40
DW02-6-4	Ca-Rds	69.80	22.83	6.90	1.47	0.32	bld	0.03	101.35
DW02-6-5	Mn-Cal	27.65	59.82	9.79	2.07	0.02	0.02	0.08	99.44
DW02-6-6	Mn-Cal	27.55	56.31	13.30	2.20	bld	bld	0.02	99.38
DW02-6-7	Mn-Cal	27.99	55.78	11.84	2.18	0.02	bld	0.07	97.88
DW03-8-1	Ca-Rds	72.00	21.73	4.12	0.65	0.18	0.01	0.07	98.76
DW03-8-2	Ca-Rds	67.43	23.90	5.21	1.71	0.18	0.02	0.51	98.95
DW03-8-3	Ca-Rds	73.15	19.40	5.73	1.38	0.32	0.07	0.68	100.73
DW03-8-4	Ca-Rds	71.30	17.65	5.67	2.35	0.17	0.02	0.66	97.82
DW03-8-5	Ca-Rds	71.60	20.18	4.67	1.23	0.22	bld	0.03	97.92
DW03-8-6	Mn-Cal	39.57	45.16	6.07	6.57	0.09	0.02	0.17	97.64
DW03-8-7	Ca-Rds	55.81	26.41	12.23	3.63	bld	0.06	0.25	98.38
DW03-8-9	Ca-Rds	67.94	17.85	5.99	5.74	0.02	0.01	2.95	100.49
DW03-8-10	Ca-Rds	68.69	22.63	6.48	2.08	0.21	bld	0.03	100.12

The contents of $MnCO_3$, $CaCO_3$, $MgCO_3$, and $FeCO_3$ are converted according to the contents of MnO, CaO, MgO, and FeO. Bdl—below detection limit. Rds—rhodochrosite, Cal—calcite.

Two samples from the Dawu deposit (DW03-1 and DW03-5) were selected for analysis of the in situ S isotope. The S isotopes of pyrite in DW03-1 vary greatly, and the $\delta^{34}S$ ranges from 23.1‰ to 56.5‰, with an average of 40.0 ± 13.4‰ (Figure 6a). However, the S isotopes of pyrite in DW03-5 are very uniform, with $\delta^{34}S$ ranging from 47.2‰ to 49.2 ‰ and an average of 48.30 ± 0.9‰ (Table 2 and Figure 6b).

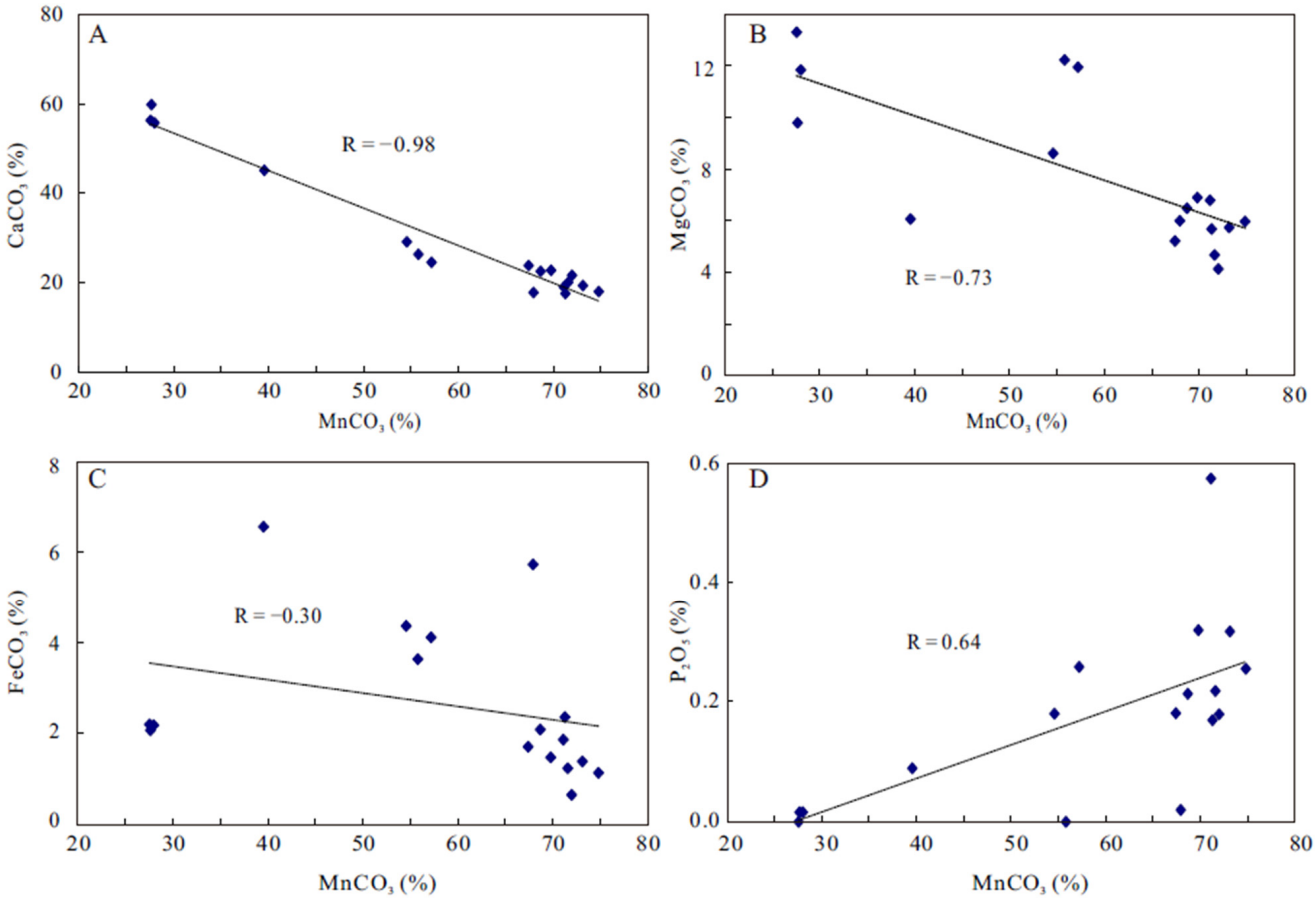

Figure 5. Correlation diagrams formajor elements of carbonates from the Dawu deposit. (**A**) $MnCO_3$ vs. $CaCO_3$; (**B**) $MnCO_3$ vs. $MgCO_3$; (**C**) $MnCO_3$ vs. $FeCO_3$; (**D**) $MnCO_3$ vs. P_2O_5.

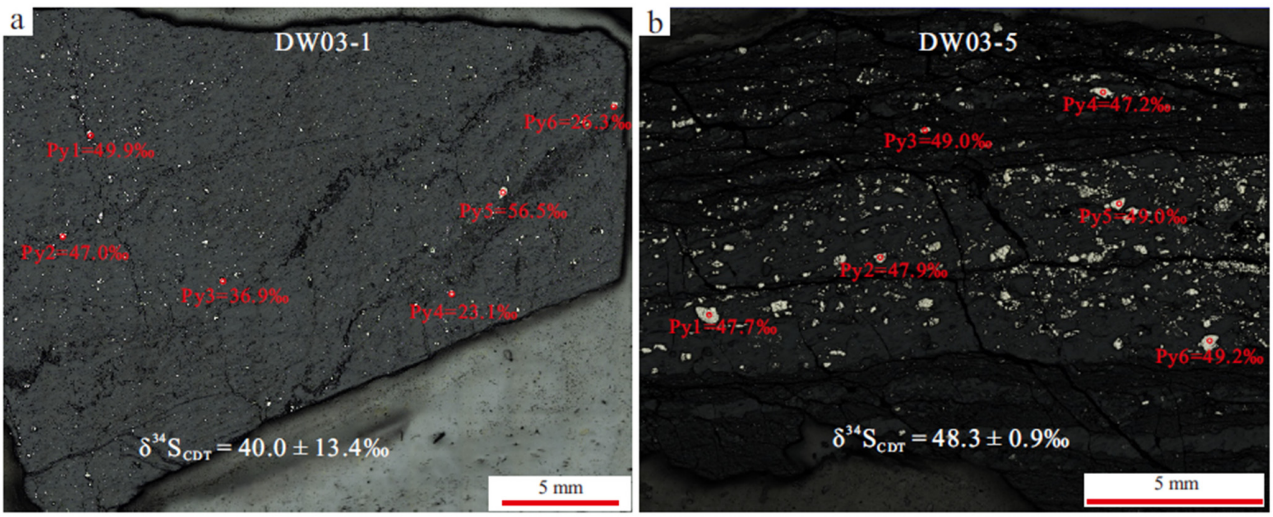

Figure 6. Analyzed points and results of the in situ sulfur isotope of pyrite from the Dawu deposit (reflected light photos, taken by a Leica DM4P optical microscope). (**a**) S isotopes of DW03-1; (**b**) S isotopes of DW03-5.

Table 2. In situ sulfur isotopic compositions of pyrite from the Dawu manganese deposit.

No.	Samples No.	$\delta^{34}S$ (‰)	$\pm 2\sigma$
1	DW03-1-Py-1	49.9	0.1
2	DW03-1-Py-2	47.0	0.2
3	DW03-1-Py-3	36.9	0.1
4	DW03-1-Py-4	23.1	0.2
5	DW03-1-Py-5	56.5	0.2
6	DW03-1-Py-6	26.3	0.2
7	DW03-5-Py-1	47.7	0.1
8	DW03-5-Py-2	47.9	0.1
9	DW03-5-Py-3	49.0	0.1
10	DW03-5-Py-4	47.2	0.1
11	DW03-5-Py-5	49.0	0.1
12	DW03-5-Py-6	49.2	0.1

6. Discussion

6.1. Separation of Mn and Fe during Sedimentation

Manganese and Fe have similar chemical properties in the supergene environment, and their separation is mainly controlled by Eh-pH conditions [42]. In the gradual oxidation of the reduced water, Fe is oxidized and precipitated before Mn, which results in the separation of Mn and Fe. When the water Eh fluctuates alternately, rhythmic layers with alternating Fe-Mn occur in the stratigraphic profile. The separation of Mn and Fe is not obvious during the rapid oxidation of water, forming Fe-Mn oxides or hydroxides [42].

The Cryogenian manganese deposits occur in the basal Datangpo Formation in South China, and no iron-rich stratum has been found in the manganese-bearing rock series or its adjacent strata [13]. The mineralization of manganese occurred after the Sturtian glaciation. The seawater under the ice sheet was in a reduced state, and Mn and Fe could accumulate as ionic compounds (Mn^{2+} and Fe^{2+}) in large quantities, which provided a material basis for the subsequent precipitation and enrichment of manganese [13,43,44]. Previous studies have shown that the Nanhua Basin was in a redox stratified environment in the Datangpo stage [45–47], and the oxidation of the water in the basin gradually increased, forming the suboxidation–oxidation environment in the shallow parts [48–50]. In the process of progressive oxidation in the marine environment after glaciation, Fe^{2+} was oxidized and precipitated before Mn^{2+}, leading to the first-stage separation of Mn and Fe [51].

The $\delta^{34}S$ values of pyrite from manganese-bearing rock series are very high, and the average $\delta^{34}S$ of pyrite in Dawu manganese deposit is 40.0–48.3‰, which is similar to the results of previous studies (Table 2 and Figure 7). This indicates that pyrite is formed in the restricted basin where sulfate consumption is much greater than supply [13,52,53], making the residual sulfate concentration extremely low and enriched in ^{34}S [54,55] and eventually forming pyrite with very high $\delta^{34}S$ [13]. There is a significant negative correlation ($R = -0.73$) between the whole-rock $\delta^{34}S$ value and S content (Figure 8B), which further indicates that the sulfate concentration in seawater should have been extremely low. The study of lithofacies paleogeography also shows that the manganese deposits were formed in the secondary Nanhua rift basins [15]. The horst formed by the extension provided a barrier for the metallogenic basin, which caused it to be a restricted basin [13,15]. The first-stage separation of Mn and Fe has occurred before the Mn-rich seawater flowing into the metallogenic basin, and the Fe was oxidized and precipitated outside the basin. Therefore, no Fe-rich stratum can be found near the Mn ore beds.

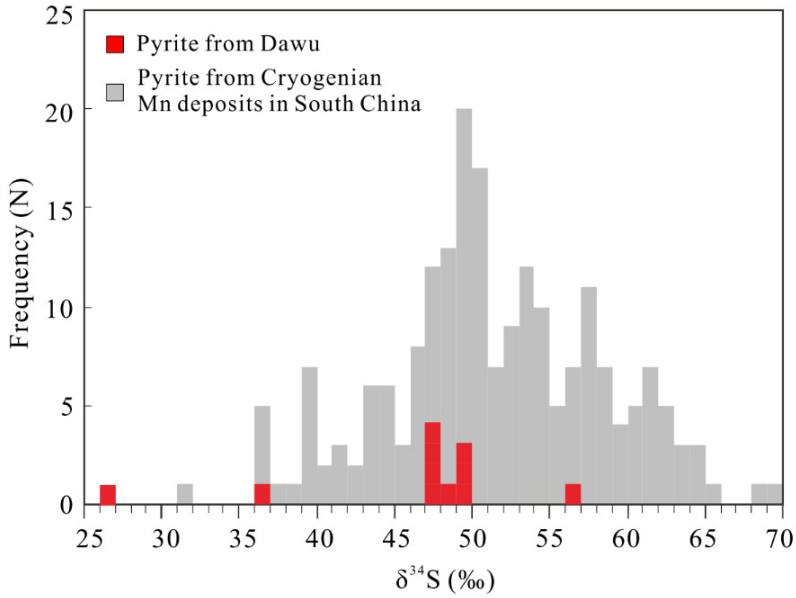

Figure 7. Histogram of sulfur isotopic compositions for pyrite from the Cryogenian manganese deposits in South China. Data of Dawu (red box) are from Table 2 of this study; data of the other deposits (gray box) are from the literature [13,33,35,37,45,54–65].

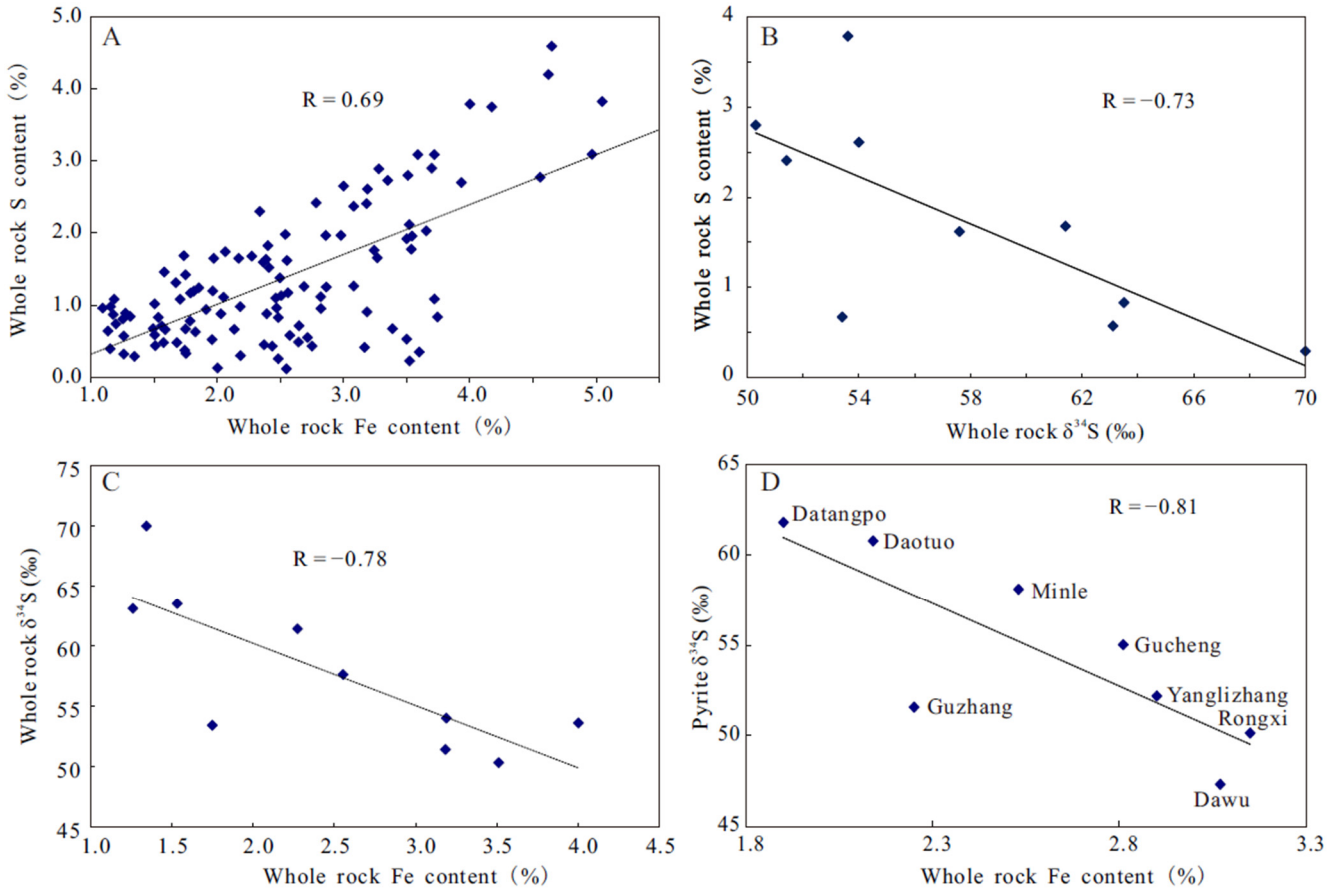

Figure 8. (**A**) Correlation diagram for whole-rock Fe and S contents from the Cryogenian manganese deposits; data are from [13,33,66]. (**B**) Correlation diagram of whole-rock $\delta^{34}S$ and S content from the Daotuo deposit; data are from [66]. (**C**) Correlation diagram of whole-rock Fe content and $\delta^{34}S$ from the Daotuo deposit; data are from [33,66]. (**D**) Correlation diagram of whole-rock Fe content and pyrite $\delta^{34}S$ from different manganese deposits; data are from [13,33].

6.2. Separation of Mn and Fe during Diagenesis

The ores from the Cryogenian manganese deposit are rich in organic matter, and Mn exists in the form of carbonates [16,38]. The manganese carbonate is depleted in ^{13}C, and $\delta^{13}C$ ranges from −6.33‰ to −10.84‰, with an average of −8.36‰, indicating that the carbon in the manganese carbonate is mainly derived from the oxidation of organic matter [38,54]. The Mn^{2+} was oxidized to Mn-oxyhydroxide in the oxic seawater and precipitated into the sediments. The buried Mn-oxyhydroxide was reduced to form Mn carbonates in the diagenetic stage [13,25,54,67,68].

There are certain differences in the whole-rock Fe content in different deposits. The highest Fe content in the Dawu and Rongxi deposits is 3.07 wt.% and 3.15 wt.%, respectively, while the lowest Fe content in Datangpo and Daotuo deposits is 1.90 wt.% and 2.14 wt.%, respectively (Figure 8D), indicating that there are differences in the separation of Mn and Fe in various deposits. The Fe mainly occurs as carbonate ($FeCO_3$) and pyrite (FeS_2) in the ores. In the manganese carbonate, Mn, Ca, Mg, and Fe exist due to isomorphic substitutions. The $MnCO_3$ is negatively correlated with $CaCO_3$ and $MgCO_3$, with correlation coefficients of −0.98 and −0.73, respectively (Figure 5A,B), while the $MnCO_3$ has no obvious correlation with $FeCO_3$ (Table 1, Figure 5C). The $FeCO_3$ content in the manganese carbonate of Dawu deposit is 0.65–6.57 wt.%, with an average of 2.63 wt.%, while that in the Datangpo deposit is 0.55–6.87 wt.%, with an average of 2.82 wt.% [38], showing no obvious difference between these two deposits.

The whole-rock Fe and S contents have a significant positive correlation (R = 0.69) (Figure 8A). Therefore, the difference in the whole-rock Fe content in the ore mainly comes from the difference in the pyrite content. Pyrite is very common in ores, showing idiomorphic–hypidiomorphic granular and framboidal textures. Pyrite nodules occur in some deposits (e.g., the Daotuo and Gucheng deposits) [66]. These pyrites can be formed in sedimentary and diagenetic stages [13]. Additionally, the whole-rock Fe content is negatively correlated with the whole-rock and pyrite $\delta^{34}S$, with correlation coefficients of −0.78 and −0.83, respectively (Figure 8C,D). There might have been a separation of Mn and Fe in the diagenetic stage, which led to the difference of whole-rock Fe content in the deposits. In the early diagenetic stage, the Mn-oxyhydroxide was reduced to Mn^{2+}, and the bicarbonate was derived from the oxidation of organic carbon, forming the manganese carbonate [67,68]. Due to the extremely low sulfate concentration in the fluid, H_2S was insufficient in the restricted basin. Therefore, the Fe^{2+} reduced in the diagenetic stage was re-released into the upper water due to the lack of H_2S, resulting in the second-stage separation of Mn and Fe and a significant negative correlation between the Fe content and $\delta^{34}S$ of the whole-rock and pyrite (Figure 8C,D).

7. Conclusions

The Cryogenian manganese deposits in South China are characterized by low Fe contents and very high $\delta^{34}S$. This study demonstrates that two-stage separations of Mn and Fe occurred during the mineralization processes. The oxidation state of seawater increased gradually after the Sturtian glaciation; therefore, Fe^{2+} was oxidized and precipitated before the Mn^{2+}, leading to the first-stage separation of Mn and Fe. The Mn-rich and Fe-poor seawater flowed into the restricted rift basin. Then, Mn and Fe were precipitated in sediments with further oxidation of the seawater. At the early stage of diagenesis, organic matter was oxidized, and Fe-Mn oxyhydroxide was reduced, forming the manganese carbonate. The H_2S was insufficient in the restricted basin due to the extremely low sulfate concentration. The Fe^{2+} was re-released due to the lack of H_2S, resulting in the second-stage separation of Mn and Fe. Finally, the manganese carbonate deposit with low Fe and extremely high $\delta^{34}S$ was formed. Therefore, the Cryogenian manganese deposits in South China are sedimentary/diagenetic-type deposits, which were formed in the restricted rift basin after the Sturtian glaciation.

Author Contributions: Conceptualization, Z.X. and C.W.; methodology, J.X.; formal analysis, X.L. and Z.J.; investigation, Z.X., C.W. and Z.Z.; resources, C.W. and Z.Z.; data curation, C.W.; writing—original draft preparation, Z.X.; writing—review and editing, C.W. and Z.Z.; supervision, Z.Z.; project administration, C.W. and Z.Z.; funding acquisition, C.W. and Z.Z. All authors have read and agreed to the published version of the manuscript.

Funding: This research was funded by the National Natural Science Foundation of China (NSFC Nos. 41703051, U1603245, and U1812402), CAS IIT (JCTD-2019-17); the Science and Technology Foundation of Guizhou Province (No. [2018] 1171); the Chinese Academy of Sciences (CAS) "Light of West China" Program; and the frontier project of the State Key Laboratory of Ore Deposit Geochemistry, Institute of Geochemistry, Chinese Academy of Sciences.

Data Availability Statement: All data generated or analyzed during this study are included in this published article.

Acknowledgments: The authors would like to thank Wei Mao and Zhuojun Xie for discussions. This manuscript greatly benefited from the valuable comments and suggestions from two anonymous reviewers and editors of Minerals.

Conflicts of Interest: This manuscript has not been published or presented elsewhere in part or in entirety, and it is not under consideration by another journal. All the authors have approved the manuscript and agree with submission to your esteemed journal. There are no conflict of interest to declare.

References

1. Taylor, S.R.; McLennan, S.M. *The Continental Crust: Its Composition and Evolution*; Blackwell: Oxford, UK, 1985; pp. 1–312.
2. Kremling, K. The behavior of Zn, Cd, Cu, Ni, Co, Fe, and Mn in anoxic baltic waters. *Mar. Chem.* **1983**, *13*, 87–108. [CrossRef]
3. Roy, S. Genetic diversity of manganese deposition in the terrestrial geological record. *Geol. Soc. Lond. Spec. Publ.* **1997**, *119*, 5–27. [CrossRef]
4. Kunzmann, M.; Gutzmer, J.; Beukes, N.; Halverson, G. Depositional environment and lithostratigraphy of the paleoproterozoic Mooidraai formation, Kalahari manganese field, South Africa. *S. Afr. J. Geol.* **2014**, *117*, 173–192. [CrossRef]
5. Beukes, N.J.; Mukhopadhyay, J.; Gutzmer, J. Genesis of high-grade iron ores of the Archean Iron Ore Group around Noamundi, India. *Econ. Geol.* **2008**, *103*, 365–386. [CrossRef]
6. Buehn, B.; Stanistreet, I.G.; Okrusch, M. Late Proterozoic outer shelf manganese and iron deposits at Otjosondu (Namibia) related to the Damaran oceanic opening. *Econ. Geol.* **1992**, *87*, 1393–1411. [CrossRef]
7. Klein, C.; Ladeira, E.A. Geochemistry and mineralogy of Neoproterozoic banded iron-formations and some selected, siliceous manganese formations from the Urucum District, Mato Grosso do Sul, Brazil. *Econ. Geol.* **2004**, *99*, 1233–1244. [CrossRef]
8. Şaşmaz, A.; Türkyilmaz, B.; ztürk, N.; Yavuz, F.; Kumral, M. Geology and geochemistry of Middle Eocene Maden complex ferromanganese deposits from the Elazığ–Malatya region, eastern Turkey. *Ore Geol. Rev.* **2014**, *56*, 352–372. [CrossRef]
9. Roy, S. Sedimentary manganese metallogenesis in response to the evolution of the Earth system. *Earth-Sci. Rev.* **2006**, *77*, 273–305. [CrossRef]
10. Johnson, J.E.; Webb, S.M.; Ma, C.; Fischer, W.W. Manganese mineralogy and diagenesis in the sedimentary rock record. *Geochim. Cosmochim. Acta* **2016**, *173*, 210–231. [CrossRef]
11. Maynard, J.B. The Chemistry of Manganese Ores through Time: A Signal of Increasing Diversity of Earth-Surface Environments. *Econ. Geol.* **2010**, *105*, 535–552. [CrossRef]
12. Krauskopf, K.B. Separation of manganese from iron in sedimentary processes. *Geochim. Cosmochim. Acta* **1957**, *12*, 61–84. [CrossRef]
13. Wu, C.; Zhang, Z.; Xiao, J.; Fu, Y.; Shao, S.; Zheng, C.; Yao, J.; Xiao, C. Nanhuan manganese deposits within restricted basins of the southeastern Yangtze Platform, China: Constraints from geological and geochemical evidence. *Ore Geol. Rev.* **2016**, *75*, 76–99. [CrossRef]
14. Zhou, Q.; Du, Y.S.; Yuan, L.J.; Zhan, S.; An, Z.Z.; Pan, W.; Yang, B.N.; Xie, X.F.; Yu, W.C.; Yin, S.L.; et al. Major progress and potential prediction of geologic exploration in Songtao manganese national fully equipped exploration district in Tongren, Guizhou. *Guizhou Geol.* **2016**, *33*, 237–244. (In Chinese with English Abstract)
15. Zhou, Q.; Du, Y.S.; Yuan, L.J.; Zhan, S.; Yu, W.C.; Yang, S.T.; Liu, Y. The structure of the Wuling rift Basin and its control on the manganese deposit during the Nanhua period in Guizhou-Hunan-Chongqing border area, South China. *Earth Sci.* **2016**, *41*, 177–188. (In Chinese with English Abstract)
16. Zhou, Q.; Du, Y.S.; Qin, Y. Ancient natural gas seepage sedimentary-type manganese metallogenic system and ore-forming model, A case study of "Datangpo type" manganese deposits formed in rift basin of Nanhua Period along Guizhou- Hunan-Chongqing border area. *Miner. Depos.* **2013**, *32*, 457–466. (In Chinese with English Abstract)

17. Li, X.H.; Li, W.-X.; Li, Z.X.; Lo, C.H.; Wang, J.; Ye, M.F.; Yang, Y.H. Amalgamation between the Yangtze and Cathaysia Blocks in South China: Constraints from SHRIMP U–Pb zircon ages, geochemistry and Nd–Hf isotopes of the Shuangxiwu volcanic rocks. *Precambrian Res.* **2009**, *174*, 117–128. [CrossRef]
18. Ye, M.F.; Li, X.H.; Li, W.X.; Liu, Y.; Li, Z.X. SHRIMP zircon U–Pb geochronological and whole-rock geochemical evidence for an early Neoproterozoic Sibaoan magmatic arc along the southeastern margin of the Yangtze Block. *Gondwana Res.* **2007**, *12*, 144–156. [CrossRef]
19. Li, Z.X.; Li, X.H.; Zhou, H.; Kinny, P.D. Grenvillian continental collision in south China: New SHRIMP U-Pb zircon results and implications for the configuration of Rodinia. *Geology* **2002**, *30*, 163–166. [CrossRef]
20. Li, Z.X.; Li, X.; Kinny, P.; Wang, J.; Zhang, S.; Zhou, H. Geochronology of Neoproterozoic syn-rift magmatism in the Yangtze Craton, South China and correlations with other continents: Evidence for a mantle superplume that broke up Rodinia. *Precambrian Res.* **2003**, *122*, 85–109. [CrossRef]
21. Wang, J.; Li, Z.X. History of Neoproterozoic rift basins in South China: Implications for Rodinia break-up. *Precambrian Res.* **2003**, *122*, 141–158. [CrossRef]
22. Wang, X.-C.; Li, X.-H.; Li, W.-X.; Li, Z.-X. Variable involvements of mantle plumes in the genesis of mid-Neoproterozoic basaltic rocks in South China: A review. *Gondwana Res.* **2009**, *15*, 381–395. [CrossRef]
23. Shu, L.S. An analysis of principal features of tectonic evolution in South China Block. *Geol. Bull. China* **2012**, *31*, 1035–1053, (In Chinese with English Abstract).
24. Jiang, G.; Sohl, L.E.; Christie-Blick, N. Neoproterozoic stratigraphic comparison of the Lesser Himalaya (India) and Yangtze block (south China): Paleogeographic implications. *Geology* **2003**, *31*, 917–920. [CrossRef]
25. Yu, W.C.; Du, Y.S.; Zhou, Q.; Wang, P.; Qi, L.; Xu, Y.; Jin, S.; Pan, W.; Yuan, L.J.; Xie, X.F.; et al. Coupling between metallogenesis of the Cryogenian Datangpo-type manganese deposit in South China and major geological events. *J. Palaeogeogr.* **2020**, *22*, 855–871. (In Chinese with English Abstract)
26. He, W.H.; Tang, T.T.; Le, M.L.; Deng, J.F.; Pan, G.T.; Xing, G.F.; Luo, M.S.; Xu, Y.D.; Wei, Y.; Zhang, Z.Y. Sedimentary and tectonic evolution of Nanhuan-Permian in South China. *Earth Sci. -J. Chian Univ. Geosci.* **2014**, *39*, 929–953. (In Chinese with English Abstract)
27. Zhou, C.; Robert, T.; Xiao, S.; Peng, Z.; Yuan, X.; Chen, Z. New constraints on the ages of Neoproterozoic glaciations in south China. *Geology* **2004**, *32*, 437–440. [CrossRef]
28. Zhang, S.; Jiang, G.; Han, Y. The age of the Nantuo Formation and Nantuo glaciation in South China. *Terra Nova* **2008**, *20*, 289–294. [CrossRef]
29. Macdonald, F.A.; Schmitz, M.D.; Crowley, J.L.; Roots, C.F.; Jones, D.S.; Maloof, A.C.; Strauss, J.V.; Cohen, P.A.; Johnston, D.T.; Schrag, D.P. Calibrating the cryogenian. *Science* **2010**, *327*, 1241–1243. [CrossRef]
30. Zhang, S.; Jiang, G.; Zhang, J.; Song, B.; Kennedy, M.J.; Christie-Blick, N. U-Pb sensitive high-resolution ion microprobe ages from the Doushantuo Formation in south China: Constraints on late Neoproterozoic glaciations. *Geology* **2005**, *33*, 473–476. [CrossRef]
31. Condon, D.; Zhu, M.; Bowring, S.; Wang, W.; Yang, A.; Jin, Y. U-Pb ages from the neoproterozoic Doushantuo Formation, China. *Science* **2005**, *308*, 95–98. [CrossRef]
32. Zhang, Q.; Chu, X.; Bahlburg, H.; Feng, L.; Dobrzinski, N.; Zhang, T. Stratigraphic architecture of the Neoproterozoic glacial rocks in the "Xiang-Qian-Gui" region of the central Yangtze Block, South China. *Prog. Nat. Sci.* **2003**, *13*, 783–787. [CrossRef]
33. Zhu, X.K.; Peng, Q.Y.; Zhang, R.B.; An, Z.Z.; Zhang, F.F.; Yan, B.; Li, J.; Gao, Z.F.; Tan, Y.; Pan, W. Geological and geochemical characteristics of the Daotuo super-large manganese ore deposit at Songtao County in Guizhou Province. *Acta Geol. Sin.* **2013**, *87*, 1335–1348. (In Chinese with English Abstract)
34. Xie, X.F.; Qin, Y.; Wen, G.G.; Xie, X.Y. Relation between Datangpo Formation and manganese mineralization in Songtao manganese mining area of Tongren in Guizhou. *Guizhou Geology* **2014**, *1*, 32–37, (In Chinese with English abstract).
35. Liu, X.F.; Wang, Q.S.; Gao, X.J. *Mangenese Deposits of Guihzou*; Guizhou People Press: Guiyang, China, 1989; pp. 1–194. (In Chinese)
36. Zhou, Q. Geological and geochemical characteristics of cold seep carbonates of Neoproterozoic Nanhua period and their significance for manganese ore deposit in east Guizhou. Ph.D. Thesis, University of Geosciences, Wuhan, China, 2008. (In Chinese with English Abstract).
37. Wang, Y.G.; Wang, L.X.; Zhu, S.C.; Xie, Z.Q.; Chen, D.C.; Zheng, S.F.; Chen, Y.L.; Zhu, H. *The Stratigrcaphy, Sedimentalry Environment and Manganese-Forming Process of Datangpo Formation in Eastern*; Guizhou People Press: Guiyang, China, 1985; pp. 1–92. (In Chinese)
38. Wu, C.Q. Geochemistry of Nanhuan Manganese Deposits in Eastern Guizhou and Adjacent Area, China. Ph.D. Thesis, University of Chinese Academy of Sciences, Beijing, China, 2016. (In Chinese with English Abstract).
39. Millet, M.-A.; Baker, J.A.; Payne, C.E. Ultra-precise stable Fe isotope measurements by high resolution multiple-collector inductively coupled plasma mass spectrometry with a 57Fe–58Fe double spike. *Chem. Geol.* **2012**, *304–305*, 18–25. [CrossRef]
40. Bao, Z.A.; Chen, L.; Zong, C.L.; Yuan, H.L.; Chen, K.Y.; Dai, M.N. Development of pressed sulfide powder tablets for in situ sulfur and lead isotope measurement using LA-MC-ICP-MS. *Int. J. Mass Spectrom.* **2017**, *421*, 255–262. [CrossRef]
41. Chen, L.; Yuan, H.; Chen, K.; Bao, Z.; Zhu, L.; Liang, P. In situ sulfur isotope analysis by laser ablation MC-ICPMS and a case study of the Erlihe Zn-Pb ore deposit, Qinling orogenic belt, Central China. *J. Asian Earth Sci.* **2019**, *176*, 325–336. [CrossRef]

42. Oztürk, M. Trends of trace metal (Mn, Fe, Co, Ni, Cu, Zn, Cd and Pb) distributions at the oxic-anoxic interface and in sulfidic water of the Drammensfjord. *Mar. Chem.* **1995**, *48*, 329–342. [CrossRef]
43. Yu, W.; Polgári, M.; Gyollai, I.; Fintor, K.; Szabó, M.; Kovács, I.; Fekete, J.; Du, Y.; Zhou, Q. Microbial metallogenesis of Cryogenian manganese ore deposits in South China. *Precambrian Res.* **2019**, *322*, 122–135. [CrossRef]
44. Yu, W.; Du, Y.; Zhou, Q. Genesis of Cryogenian Datangpo manganese deposit: Hydrothermal metal inputs and episodic post-glacial ventilation of Nanhua basin, South China. *Palaeogeogr. Palaeoclimatol. Palaeoecol.* **2016**, *459*, 321–337. [CrossRef]
45. Li, C.; Love, G.D.; Lyons, T.W.; Scott, C.T.; Feng, L.; Huang, J.; Chang, H.; Zhang, Q.; Chu, X. Evidence for a redox stratified Cryogenian marine basin, Datangpo Formation, South China. *Earth Planet. Sci. Lett.* **2012**, *331*, 246–256. [CrossRef]
46. Wei, W.; Wang, D.; Li, D.; Ling, H.; Chen, X.; Wei, G.; Zhang, F.; Zhu, X.; Yan, B. The marine redox change and nitrogen cycle in the Early Cryogenian interglacial time: Evidence from nitrogen isotopes and Mo contents of the basal Datangpo Formation, northeastern Guizhou, South China. *J. Earth Sci.* **2016**, *27*, 233–241. [CrossRef]
47. Xu, L.; Frank, A.B.; Lehmann, B.; Zhu, J.; Mao, J.; Ju, Y.; Frei, R. Subtle Cr isotope signals track the variably anoxic Cryogenian interglacial period with voluminous manganese accumulation and decrease in biodiversity. *Sci. Rep.* **2019**, *9*, 1–8. [CrossRef] [PubMed]
48. Zhang, F.; Zhu, X.; Yan, B.; Kendall, B.; Peng, X.; Li, J.; Algeo, T.J.; Romaniello, S. Oxygenation of a Cryogenian ocean (Nanhua Basin, South China) revealed by pyrite Fe isotope compositions. *Earth Planet. Sci. Lett.* **2015**, *429*, 11–19. [CrossRef]
49. Ai, J.; Zhong, N.; Zhang, T.; Zhang, Y.; Wang, T.; George, S.C. Oceanic water chemistry evolution and its implications for post-glacial black shale formation: Insights from the Cryogenian Datangpo Formation, South China. *Chem. Geol.* **2021**, *566*, 120083. [CrossRef]
50. Hohl, S.V.; Jiang, S.-Y.; Viehmann, S.; Wei, W.; Liu, Q.; Wei, H.-Z.; Galer, S.J. Trace Metal and Cd Isotope Systematics of the Basal Datangpo Formation, Yangtze Platform (South China) Indicate Restrained (Bio) Geochemical Metal Cycling in Cryogenian Seawater. *Geosciences* **2020**, *10*, 36. [CrossRef]
51. Wu, C.Q.; Zhang, Z.W.; Xiao, J.F.; Xu, J.H.; Li, X.Y.; Jin, Z.R. The study of separation mechanism of manganese and iron in Cryogenian manganese deposit, Eastern Guizhou, China. In Proceedings of the 9th National Symposium on Metallogenic Theory and Prospecting Methods, Nanjing, China, 13 December 2019; pp. 112–113.
52. Wu, C.; Zhang, Z.; Zheng, C.; Yao, J. Implication of Ultra-high δ 34 S Values in Pyrite from Manganese Deposits of the Datangpo Stage, Yangtze Platform, China. *Acta Geol. Sin.* **2014**, *88*, 266–267. (In Chinese) [CrossRef]
53. Wu, C.Q.; Cheng, Y.; Zhang, Z.W.; Xiao, J.F.; Fu, Y.Z.; Shao, S.X.; Zheng, C.F.; Yao, J.H. Geological implications of ultra-high δ 34 S values of pyrite in manganese deposits of Nanhua Period in eastern Guizhou and adjacent areas, China. *Geochimica* **2015**, *44*, 213–224. (In Chinese with English Abstract)
54. Pei, H.X.; Li, Y.H.; Fu, Y.; Zhan, M.C. Metallogenic mechanism of "Datangpo Type" manganese deposits in Gaodi, Guizhou Province: Constrains from sulfur and carbon iIsotopes. *Acta Geosci. Sin.* **2020**, *41*, 651–662. (In Chinese with English Abstract)
55. Wang, P.; Algeo, T.J.; Zhou, Q.; Yu, W.; Du, Y.; Qin, Y.; Xu, Y.; Yuan, L.; Pan, W. Large accumulations of 34S-enriched pyrite in a low-sulfate marine basin: The Sturtian Nanhua Basin, South China. *Precambrian Res.* **2019**, *335*, 105504. [CrossRef]
56. Tang, S.Y. Isotopic geological study of manganese deposit in Minle area, Hunan Province. *Acta Sedimentol. Sin.* **1990**, *8*, 77–84. (In Chinese with English Abstract)
57. Li, R.W.; Zhang, S.K.; Lei, J.J.; Shen, Y.A.; Chen, J.S.; Chu, X.L. Temporal and spacial varation in δ34S values of pyrite from Sinian strata discussion on relationship between Yangtze Block and the late Proterozoic supercontinental. *Chin. J. Geol.* **1996**, *31*, 209–217. (In Chinese with English Abstract)
58. Li, R.W.; Chen, J.; Zhang, S.; Lei, J.; Shen, Y.; Chen, X. Spatial and temporal variations in carbon and sulfur isotopic compositions of Sinian sedimentary rocks in the Yangtze platform, South China. *Precambrian Res.* **1999**, *97*, 59–75. [CrossRef]
59. Chu, X.L.; Li, R.W.; Zhang, T.G.; Zhang, Q.R. Implication of ultra-high δ34S values of pyrite in manganese mineralization meds of Datangpo stage. *Bull. Mineral. Petrol. Geochem.* **2001**, *20*, 320–322. (In Chinese with English Abstract)
60. Feng, L.-J.; Chu, X.-L.; Huang, J.; Zhang, Q.-R.; Chang, H.-J. Reconstruction of paleo-redox conditions and early sulfur cycling during deposition of the Cryogenian Datangpo Formation in South China. *Gondwana Res.* **2010**, *18*, 632–637. [CrossRef]
61. Zhang, F.F.; Zhu, X.K.; Gao, Z.F.; Cheng, L.; Peng, Q.Y.; Yang, D.Z. Implication of the precipitation mode of manganese and ultra-high δ34S values of pyrite in Mn-carbonate of Xixibao Mn ore deposit in northeastern Guizhou Province. *Geol. Rev.* **2013**, *59*, 274–286. (In Chinese with English Abstract)
62. Liu, T.-B.; Maynard, J.B.; Alten, J. Superheavy S isotopes from glacier-associated sediments of the Neoproterozoic of south China: Oceanic anoxia or sulfate limitation? In *Evolution of Early Earth's Atmosphere, Hydrosphere, and Biosphere—Constraints from Ore Deposits*; Kesler, S.E., and Ohmoto, H., Eds.; Geological Society of America Memoirs: Boulder, CO, USA, 2006; Volume 198, pp. 205–222.
63. Zhang, T.G.; Chu, X.L.; Feng, L.J.; Zhang, Q.R.; Guo, J.P. The effects of the Neoproterozoic Snowball Earth on carbon and sulfur isotopic compositions in seawater. *Acta Geosci. Sin.* **2003**, *24*, 487–493. (In Chinese with English Abstract)
64. Tang, S.; Liu, T. Origin of the early Sinian Minle manganese deposit, Hunan Province, China. *Ore Geol. Rev.* **1999**, *15*, 71–78. [CrossRef]
65. Wang, P.; Zhou, Q.; Du, Y.S.; Yu, W.C.; Xu, Y.; Qi, L.; Yuan, L.J. Characteristics of pyrite sulfur isotope of Mn deposit from Datangpo Formation in the Songtao area, East Guizhou Province and its geological significance. *Earth Sci.* **2016**, *41*, 2031–2040. (In Chinese with English Abstract)

66. Zhang, F.F. The Formation Mechanism of Datangpo Manganese Ore Deposits during Nanhua Period in South China and the Paleo-Redox Conditions of Nanhua Marine Basin. Master's Thesis, Chinese Academy of Geological Sciences, Beijing, China, 2014. (In Chinese with English Abstract).
67. Kuleshov, V.N. Manganese deposits: Communication 1. Genetic models of manganese ore formation. *Lithol. Miner. Resour.* **2011**, *46*, 473–493. [CrossRef]
68. Kuleshov, V.N. *Isotope Geochemistry: The Origin and Formation of Manganese Rocks and Ores*; Elsevier: Amsterdam, The Netherlands, 2017; pp. 1–427.